PROCEEDINGS OF SPIE

Ground-based coronagraphy with high-order adaptive optics

Russell B. Makidon, Anand Sivaramakrishnan, Christopher D. Koresko, Thomas Berkefeld, Marc J. Kuchner, et al.

SPIE.

Ground-Based Coronagraphy with High Order Adaptive Optics

Russell B. Makidon[a], Anand Sivaramakrishnan[a], Christopher D. Koresko[b],
Thomas Berkefeld[c], Marc J. Kuchner[d] and Robert Winsor[a]

[a]Space Telescope Science Institute, 3700 San Martin Drive,
Baltimore MD 21218, USA
[b] Division of Geology and Planetary Sciences, California Institute of Technology
Pasadena, CA 91125, USA
[c] Max-Planck Institut fur Astronomie, Koenigstuhl, Heidelberg, Germany
[d] Palomar Observatory, California Institute of Technology
Pasadena, CA 91125, USA

ABSTRACT

We simulate the actions of a coronagraph matched to diffraction-limited adaptive optics (AO) systems on the Calypso 1.2m, Palomar Hale 5m and Gemini 8.1m telescopes, and identify useful parameter ranges for AO coronagraphy on these systems. We model the action of adaptive wavefront correction with a tapered, high-pass filter in spatial frequency rather than a hard low frequency cutoff, and estimate the minimum number of AO channels required to produce sufficient image quality for coronagraphic suppression within a few diffraction widths of a central bright object (as is relevant to *e.g.*, brown dwarf searches near late-type dwarf stars). We explore the effect of varying the occulting image-plane stop size and shape, and examine the trade-off between throughput and suppression of the image halo and Airy rings. We discuss our simulations in the context of results from the 241-channel Palomar Hale AO coronagraph system, and suggest approaches for future AO coronagraphic instruments on large telescopes.

Keywords: diffraction-limited imaging, coronagraphy, adaptive optics, high dynamic range imaging

1. INTRODUCTION

An imaging coronagraph used in conjunction with an adaptive optics (AO) system can improve the sensitivity of an imaging system to faint structure surrounding a bright source. This device blocks the core of the image of an on-axis point source and suppresses the bright inner diffraction rings and halo, removing light which might otherwise saturate a detector and reduce the dynamic range of the imaging before faint off-axis structure can be discerned. The choice of pupil plane and image plane stops sizes can only be made by understanding image formation by the AO system and the interaction between the AO system and the coronagraph.

With an AO system in place, the image plane stop can be made very small: only slightly larger than than the diffraction spot itself. However, a pupil-plane stop matched to a small occulting image-plane stop must have a small diameter to significantly reduce the off-axis throughput. There is a trade-off between throughput and scattered-light suppression. In some situations using a coronagraph does not improve the final dynamic range of an instrument.

To address this issue, we simulated image formation in a coronagraph mounted on a telescope with an AO system and investigated the effects of atmospheric turbulence under a range of seeing conditions, telescope sizes, and AO system performance levels. We present our results in a form that should be useful both for the designer of such a system and for potential users. We discuss the results of the simulations in the context of current and next-generation instruments. Oppenheimer *et al.*[1] investigated these trade-offs observationally using the Palomar AO coronagraph. We briefly discuss their observations in the context of this work.

Our model is an extension of that of Nakajima,[2] who modelled low order ground-based AO coronagraphs and simulated the AO wavefront correction by zeroing out the lowest order Zernike coefficients in the expression used to generate realizations of Kolmogorov fluctuations in the atmosphere's refractive index. In Nakajima's work, the

(Send correspondence to A.S. — e-mail: anands@stsci.edu)

Lyot stop is "oversized" by a fixed amount (10% of the pupil diameter), and occulting image-plane stop sizes are chosen to be 1, 5, 10 and 15 times the telescope resolution. We extend Nakajima's approach in four ways. First, we match the Lyot stop oversizing to the size of the image-plane stop to optimize coronagraphic performance. Second, we use a graded high-pass filter to mimic AO correction. Third, we investigate higher order adaptive correction of the incoming wavefront to model AO systems with a few thousand actuators. We concentrate on the smallest stop sizes allowed by Fourier optics that do not lead to an unacceptable reduction in throughput: between 3 and 6 λ/D radians. Finally, we employ a rapid Markov algorithm (Glindemann et al.[3] to realize the Kolmogorov-spectrum phase screens used to simulate atmospheric effects (Berkefeld[4]).

2. NUMERICAL SIMULATIONS

We simulate the performance of coronagraphs and AO systems on three ground-based telescopes: the Calypso 1.2m at Kitt Peak, the Palomar Hale 5m and the Gemini 8.1m. We simulate a monolithic circular aperture with its secondary obstruction, oversampling the resultant image by a linear factor of 4 to 8 in order to achieve sub-diffraction-width resolution. We do not include the effects of spiders, mirror surface micro-roughness, or internal scattering in the current simulations. We only model moderate to good seeing conditions appropriate for each telescope (taking into account the target imaging wavelengths). Seeing is characterized by the value of D/r_0 used to generate phase screens, where r_o is the value of Fried's parameter (Fried[5]) that describes the spectrum of the phase of the wavefront, and D is the telescope diameter.

In this analysis, we consider only monochromatic imaging, but note that in typical broad-band imaging, the final image can be described by the sum or integral of several monochromatic images weighted by the instrumental transmission function. Wavelength variation across the band will act in such a way as to smear image features radially by the same factor as the fractional bandwidth, since the wavelength enters into diffraction-limited image formation only in the combination (λ/D). Hence bright Airy rings will get wider, but coronagraphic suppression of such rings will persist. By treating the monochromatic case we can distinguish between halo suppression and Airy ring suppression.

On Calypso and Gemini we explored the degree of correction required to make coronagraphic imaging profitable, and used the smallest AO system that achieved this purpose. For the Hale 5m simulations we used an actuator density corresponding to the Cassegrain 241-channel AO system currently in place. We also simulated an actuator density corresponding to 431 channels of adaptive correction on the Hale. We use the AO system's Strehl ratio as a parameter to compare these simulations with existing or proposed AO systems. The Strehl ratio of an imaging system is the ratio of actual peak intensity in the image to the peak intensity the system would produce in the absence of all wavefront aberration. It must be borne in mind that the Strehl ratio will be a function of the brightness of the on-axis object being occulted by the coronagraphic imaging stop. We estimate the total number of AO channels in a system, N_{tot}, from the number of actuators across the primary, N (which we specify), with the approximation

$$N_{tot} = \pi(N/2)^2, \tag{1}$$

without taking secondary obscurations, detailed edge effects or exact actuator placement into consideration.

2.1. *AO* correction

We generate realizations of phase screens with Kolmogorov spectra to create static input phase screens representing the wavefronts that illuminate the primary aperture of the coronagraph.

For our purposes, input to this code consists of the size of the square array of desired phase values, and the value of r_o. We also generate 'sub-harmonic' frequencies that represent phase variations larger than the primary diameter, though these are essentially removed by the simulated AO correction.

The maximum angular extent of the final simulated images using the Kolmogorov phase screens is determined by the resolution of the phase screen grid (*i.e.*, the number of 'pixels' across the telescope aperture). For this analysis, we used phase screens with resolutions considerably finer than the turbulence scale length r_0 — our coarsest sampling is 17 pixels/r_0 for Gemini with $D/r_0 = 30.0$, and our finest sampling is 30 pixels/r_0 for Calypso with $D/r_0 = 5.0$. In the image plane, the inverse of the phase screen grid size (measured in wavelengths) is a larger angle than any of the image profile plots we present. Hence we can be reasonably sure that our phase screen discretization introduces no artifacts in the regions of interest.

400

An ideal *AO* system would remove all but the DC power from the incoming wave's phase. However, real *AO* systems cannot make corrections on scales finer than the inter-actuator spacing. This limitation causes an *AO* system to behave as a high-pass filter: it attenuates power in the phase function at low spatial frequencies.

We model the effect of *AO* with a Hanning filter whose cutoff frequency corresponds to the Nyquist frequency of the actuator system. This spatial frequency is $k_{max} = \lambda/(2D_{actuator})$, where $D_{actuator}$ is the inter-actuator spacing (or equivalently, $k_{max} = N\lambda/2D$, where N is the number of actuators across the primary diameter). The smooth taper of the Hanning filter is an attempt to mimic the smooth degradation of the *AO* correction with increasing spatial frequency. Individual *AO* systems will all have slightly different filter representations, but this model tries to reproduce the essential character of astronomical *AO* with a finite number of channels.

We multiply the Fourier transform of the phase array by the complement of the Hanning shading function,

$$
\begin{aligned}
A(k) &= 1 - \tfrac{1}{2}(1 + cos(\pi k/k_{max})), &&\text{for } k < k_{max} \\
A(k) &= 1, &&\text{otherwise,}
\end{aligned}
\tag{2}
$$

and inverse-transform the product to create a corrected phase screen. We perform this filtering on a phase array twice the linear size of the primary to ensure that edge effects of the high pass filtering do not affect the phase array over the primary, and we use the central portion of the resultant phase array as the phase function, ϕ, on the telescope primary.

2.2. Coronagraphic optics

We place our *AO*-corrected phase screen on the telescope aperture, and embed this in the middle of a zero-filled square array with a side 4 to 8 times the telescope aperture diameter. This produces a resolution of 4 to 8 samples across each optical resolution element (of size λ/D) in our images. Given our oversampling of the aperture plane — a factor of 4 for the Gemini simulations, and a factor of 8 for the Palomar Hale and Calypso simulations — the image plane stops we model have at least 16 samples across them. When computer memory limits our oversampling to a factor of 4 (in the Gemini simulations) the smallest stop we model has a diameter of $4\lambda/D$ radians. When the oversampling is a factor of 8, our smallest stop is $3\lambda/D$ across.

We transform the corrected phase screen over the primary to create the first image plane field, and then simulate a hard-edged ("top hat") or graded ("fez") coronagraphic stop in the image plane. We measure the stop sizes by their $FWHM$ in units of λ/D. The fez stop profile function is shown in Figure 1. The central regions of these stops are fully opaque, which reduces the effects of guiding and centering errors.

In order to compare stops of different shapes we calculated the fraction of the image flux that is blocked by the occulting image-plane stop. We find that a fez is slightly more efficient at blocking on-axis source flux than a top hat of the same $FWHM$, especially for the smaller stops used in our investigation.

This stopped image is propagated to the next pupil plane, where the Lyot stop is located. In real instruments this is accomplished with more optics. Here we simply inverse-transform the occulted image field.

When the incoming wavefront is perfectly flat, the natural scale for the radius of the Lyot stop is $D/2 - D/s$, where D is the telescope aperture diameter and s is the width of the image-plane spot in units of λ/D. In general, however, the Lyot stop that offers the most useful combination of throughput and suppression of the on-axis source will have a radius of $D/2 - \mathcal{F}D/s$, where $\mathcal{F}$ is a factor of order unity (Sivaramakrishnan *et al.*[6]). We call $\mathcal{F}$ the "Lyot fine tuning parameter".

Inspection of the energy distribution in the Lyot plane from an on-axis source shows that $\mathcal{F} = 1$ causes a reduction in throughput without improving on-axis energy suppression much when compared to smaller values of $\mathcal{F}$: smaller values provide almost as much coronagraphic suppression but allow for more throughput of off-axis light. In this study we used two values of $\mathcal{F}$ — 0.25 and 0.5 — in all our simulations. When designing a real diffraction-limited coronagraph for a particular telescope, values of $\mathcal{F}$ can be examined on a finer grid. There may also be instrument-specific reasons (scatter, imperfect DM control, etc.) for making $\mathcal{F}$ slightly larger than the theoretically optimal value. These parameters pertain to the image-plane stop diameters used in this work (*e.g.*, $3\lambda/D$ to $6\lambda/D$).

For the smaller image-plane stops, the difference in Lyot stop throughput between the values we use is sometimes significant. The smaller the value of $\mathcal{F}$, the more scattered light from aperture boundaries or discontinuities gets to the final image, so the trade-off in the choice of $\mathcal{F}$ is dynamic range against throughput. This trickles down to signal-to-noise ramifications when planning coronagraphic observations.

We apply this matched Lyot stop to the pupil field, and perform a last Fourier transform on this field to produce the final image. We ran our simulations on a Sun Ultra 60. An 8.1m aperture coronagraphic simulation in IDL ran in five minutes. Generating the input phase screens (which were saved on disk) required minimal computing resources compared to the coronagraph optics simulation.

3. DISCUSSION

We chose to simulate three aperture classes. The smallest aperture simulated is that of Calypso, which has a 1.2m diameter aperture with a central obscuration diameter of 30% of the primary diameter. This telescope has arguably the best control of ground seeing of any small aperture telescope, and was constructed specifically to minimize scatter (Smith[7]). The large central obscuration does limit its diffraction-limited coronagraphic performance somewhat, but the real limit to the utility of high order AO on such telescopes is due to their small collecting area. In order for AO to suppress the wings in the image, there have to be many wavefront sensing channels across the mirror. That requirement places a severe constraint on the brightness of usable targets for AO. The mid-sized telescope we simulated is the 5m diameter Hale, since it has an existing AO system and coronagraph. The central obscuration diameter is 36% of the primary diameter. We matched the Strehl ratio of our simulations to a range of values that are produced by the Hale AO system. The largest aperture considered is the 8m Gemini design. A near infrared coronagraph is being designed for that telescope, and we wished to outline some profitable areas of AO coronagraph parameter space for such an instrument. We present simulated examples of companion objects with and without an AO coronagraph in section 3.3. For Gemini, we used an obscuration diameter that is 13% of the aperture diameter.

3.1. Kitt Peak Calypso 1.2m telescope

For our simulations of the Calypso 1.2m telescope on Kitt Peak — a telescope where tip-tilt effects are the dominant source of atmospheric aberration — we investigated two seeing conditions: $r_0 = 0.40m$ and $r_0 = 0.24m$, yielding D/r_0 values of 3.0 and 5.0 respectively. These choices were predicated on the assumption of "upper quartile" and typical seeing values for this telescope in the longer optical bandpasses (Smith[7]).

To determine when AO corrections became important, we varied the number of AO correction channels until we recovered structure in the Airy rings. With 38 channels of AO (distributed uniformly across the primary), we expect Strehl ratios as high as 60%.

Table 1. Calypso 1.2m Telescope: Simulated Strehl Ratios

Atmosphere	Number of Actuators Across Pupil Diameter				
	No AO	7 Actuators	11 Actuators	15 Actuators	23 Actuators
$D/r_0 = 3.0$	0.55	0.80	0.90	0.94	0.97
$D/r_0 = 5.0$	0.23	0.61	0.78	0.87	0.93

The grid of simulated $PSFs$ is shown in Figure 2. In this case the primary effect of a coronagraph is the suppression of the Airy rings out to many diffraction widths. The broad underlying halo is not suppressed a few resolution elements past the image-plane stop, as this halo is unaffected by AO correction. A dynamic range increase of about a factor of 3 results from the Airy ring suppression in the monochromatic case. With broad-band ($\delta\nu/\nu \sim 50\%$) imaging this will result in somewhat smaller intensity suppression over more of the image, since Airy rings will be suppressed but underlying halo will not.

We see suppression by factors of 3-6 within two Airy rings of the field stop edge. There is little to be gained by grading the edge of the image-plane stop. When the occulting stop is smaller than $\sim 3\lambda/D$ in diameter, scatter from the primary perimeter and secondary obstruction fills the pupil with light, and coronagraphic optics cease to provide any benefit (especially with the large secondary obstruction).

3.2. Palomar Hale 5m telescope

The AO system currently in use at the Hale 5m telescope has 16 actuators across the primary diameter. We match this actuator density in our simulations, which produce Strehl ratios of $\sim 70\%$ with $D/r_0 = 10$. At this image quality, coronagraphic imaging does not produce significant suppression in the wings of the image, though a little

Table 2. Coronagraph Simulations: Calypso 1.2m Telescope

Image Stop Diameter	Lyot Throughput		$D/r_0 = 3$ % PSF Blocked		$D/r_0 = 5$ % PSF Blocked	
	$\mathcal{F} = 0.25$	$\mathcal{F} = 0.50$	Top hat	Fez	Top hat	Fez
$3\lambda/D$	0.60	0.26	58	63	46	51
$4\lambda/D$	0.70	0.42	74	75	60	61
$5\lambda/D$	0.75	0.53	78	80	65	68
$6\lambda/D$	0.79	0.60	81	82	71	73

Simulations assume an AO system of 7 actuators across the pupil diameter

Airy ring suppression out to $8\lambda/D$ is seen. When we increased the number of AO channels to 23 across the primary (which doubles the number of AO channels), the Strehl ratio produced by the simulated AO system rose to 81%. At these Strehl ratios, a stop of $4\lambda/D$ with $\mathcal{F} = 0.5$ produced threefold Airy ring suppression out to the bright ring at $6\lambda/D$. Azimuthally averaged PSFs for the Hale are shown in Figure 3.

Table 3. Palomar Hale 5m Telescope: Simulated Strehl Ratios

Atmosphere	Number of Actuators Across Pupil Diameter				
	No AO	16 Actuators	23 Actuators	51 Actuators	99 Actuators
$D/r_0 = 10.0$	0.06	0.70	0.81	0.94	0.98
$D/r_0 = 20.0$	0.03	0.29	0.52	0.84	0.94

Oppenheimer *et al.*[1] finds that for a 50% Strehl ratio on the Palomar AO system (in K) and a spot size of $9\lambda/D$, a Lyot stop with $\mathcal{F} = 0.9$ was considerably more effective than one with $\mathcal{F} = 0.45$. We have not simulated such large field stops, though the observational result indicates that such configurations merit attention. We note that for larger values of the image-plane stop diameter s (measured in units of λ/D), the throughput penalty of larger values of $\mathcal{F}$ is reduced, so the optimal value of $\mathcal{F}$ is expected to grow with s.

Table 4. Coronagraph Simulations: Palomar Hale 5m Telescope

Image Stop Diameter	Lyot Throughput		$D/r_0 = 10$ % PSF Blocked		$D/r_0 = 20$ % PSF Blocked	
	$\mathcal{F} = 0.25$	$\mathcal{F} = 0.50$	Top hat	Fez	Top hat	Fez
$3\lambda/D$	0.59	0.25	48	53	23	25
$4\lambda/D$	0.69	0.41	61	62	30	31
$5\lambda/D$	0.75	0.52	64	65	33	34
$6\lambda/D$	0.79	0.59	65	66	36	36

Simulations assume an AO system of 16 actuators across the pupil diameter

3.3. Gemini 8.1m telescope

The smallest AO system that made a qualitative difference to coronagraphic suppression in moderate seeing ($D/r_o = 30$, as might be expected in the J band) has 51 actuators across the primary diameter, or about 2000 channels. We know of at least two efforts to fabricate deformable mirrors that might be used in such systems (Langlois et al.,[8] and Winsor et al.[9]). With such a system we simulated stops of 4, 5 and 6 λ/D. We found that the smallest stop worked best: larger stops did not improve the suppression — they simply obscured bigger area around the central object.

When $D/r_0 = 30$ we estimate a Strehl ratio of 68% from the AO system. In this case we found central object suppression of factors of three between bright Airy rings, and ten at the rings (see Figure 4). The Lyot stop fine

Table 5. Gemini 8.1m Telescope: Simulated Strehl Ratios

Atmosphere	Number of Actuators Across Pupil Diameter			
	No AO	25 Actuators	51 Actuators	99 Actuators
$D/r_0 = 15.0$	0.05	0.70	0.89	0.96
$D/r_0 = 22.5$	0.01	0.43	0.79	0.93
$D/r_0 = 30.0$	0.01	0.26	0.68	0.88

tuning factor $\mathcal{F}$ of 0.5 worked a little better than the smaller value of 0.25, especially at the smallest stop size. We found no noticeable difference between a graded occulting stop and a hard-edged one.

When $D/r_o = 15$ (e.g., in the K band), coronagraphic performance improves dramatically. In this case the AO system delivers a Strehl ratio of 90%. We see bright ring suppression of a factor of three at $7.5\lambda/D$, but the most dramatic ring suppression is a factor of over 10 or more in the Airy rings located at 3.5 and 5.5 λ/D (Figure 4). We also see suppression by factors of about 3 in the dark rings.

A stop size of $4\lambda/D$ or smaller, with a Lyot stop fine tuning factor $\mathcal{F}$ of 0.5 looks like a very good starting point for further investigation for an AO coronagraph optimized for the best seeing on Gemini. In Figure 5 we show simulated images for companions with brightness differences Δm of +5, +7.5 and +10 magnitudes relative to the primary object. In the absence of noise, we see that at a companion with $\Delta m = +7.5$ in $H-$band at a separation of 0.16 arcseconds is observable under good seeing conditions ($D/r_o = 15$) when using 2000 channel AO coronagraph with a 0.16 arcsecond diameter field stop. However, scattered light from the occulted primary star is of comparable brightness. In this realization, the +10 magnitude companion is not discernible above the scattered light from the primary, though with long integration times such a companion may prove to be detectable.

Table 6. Coronagraph Simulations: Gemini 8.1m Telescope

Image Stop Diameter	Lyot Throughput		$D/r_0 = 15.0$ % PSF Blocked		$D/r_0 = 22.5$ % PSF Blocked		$D/r_0 = 30.0$ % PSF Blocked	
	$\mathcal{F} = 0.25$	$\mathcal{F} = 0.50$	Top hat	Fez	Top hat	Fez	Top hat	Fez
$4\lambda/D$	0.76	0.55	79	80	70	70	60	61
$5\lambda/D$	0.80	0.63	81	81	71	72	62	62
$6\lambda/D$	0.83	0.68	82	82	73	73	63	63

Simulations assume an AO system of 51 actuators across the pupil diameter

3.4. General Comments

The advantage of coronagraphic imaging is concentrated in an area just outside the image stop, except when tip-tilt is the dominant wavefront aberration. In order to make best use of a high order AO coronagraph, the stop sizes and target object separations should be closely linked. When small image-plane stops are used the Lyot stop size must be carefully chosen to find the best trade-off between throughput and image suppression. One somewhat surprising result of this study is the fact that such instruments might work quite well in the shorter wavelength bands on large telescopes.

We concentrated on simple stop shapes because we felt that a reflective surface (such as the glass on which a Gaussian spot might lie) in an image plane would be the source of too much scattered light and ghosting, even though a Gaussian spot is optimal from a theoretical standpoint. Solid occulting stops would certainly have sufficient attenuation of the central object. Variably-sized Lyot stops such as multiple leaf diaphragms could be utilized if they do not complicate the PSF too much.

For 1-m class telescopes in optical wavelengths, we find that AO systems with 7 actuators across the primary get $\sim$ 60% Strehl ratios without compromising the brightness limits of available AO targets excessively (e.g. 30

parsecs for an M0 star), but only modest contrast ratio gains are achieved with a coronagraph. The coronagraphic suppression is evident only in the bright Airy rings of the image.

For 5-m class telescopes the current 241-actuator Palomar AO system is a useful for coronagraphy. Stop sizes down to $3\lambda/D$ are workable, though most of the coronagraphic benefit is seen in bright ring suppression. However, if the number of actuators were doubled such telescopes would routinely produce Strehl ratios around 80% (with a $\sim$ 40 parsec limit on an M0 AO guide star). In this case coronagraphic suppression improves dramatically. In addition to the bright ring suppression, image halo suppression starts to be seen just outside the image-plane stop. The biggest gains are to be found in the longer near-IR bands H and K.

On 8-m class telescopes coronagraphic gains are to be found with 2000 actuator AO systems, stop sizes can be at least as small as $4\lambda/D$, and halo suppression of a factor of 3 is seen in the vicinity of the stop edge. Coronagraphic AO will work well in the J, H and K bands.

ACKNOWLEDGMENTS

REFERENCES

1. Oppenheimer, B. R., Dekany, R., Hayward, T., Brandl, B & Troy, M. 2000, SPIE Conference procedings, Munich.
2. Nakajima, T. 1994, ApJ, 425, 348.
3. Glindemann, A., Lane, R. G. & Dainty, J. C. 1993, Journal of Modern Optics, 40, 2381
4. Berkefeld, T. 1999, private communication.
5. Fried, D. L. 1966, JOSA, 56, 1372
6. Sivaramakrishnan, A., Koresko, C. D., Makidon, R. B., Berkefeld, T. & Kuchner, M. J. 2000, in preparation.
7. Smith, E. 1999, Ph. D. thesis, Columbia University.
8. Langlois, M. P., Angel, J. R. P., Lloyd-Hart, M., Miller, S. & Angeli, G. 1999, SPIE Conference procedings v.3762, Denver.
9. Winsor, R., Sivaramakrishnan, A., & Makidon, R. 2000, SPIE Conference procedings, Munich.
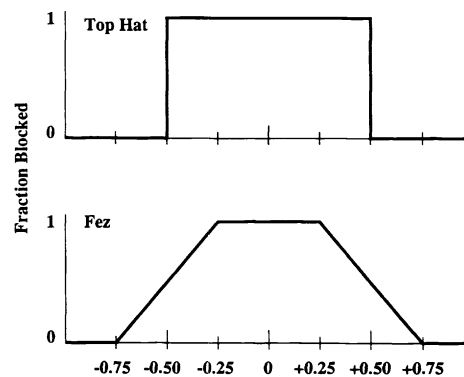
Figure 1. Profiles of top hat and fez image-plane stop shapes with the same $FWHM$. The fez function is unity out to a radius of 0.25, and decreases linearly to zero at a radius of 0.75.

Simulated Calypso Point Spread Functions: Tophat Stop
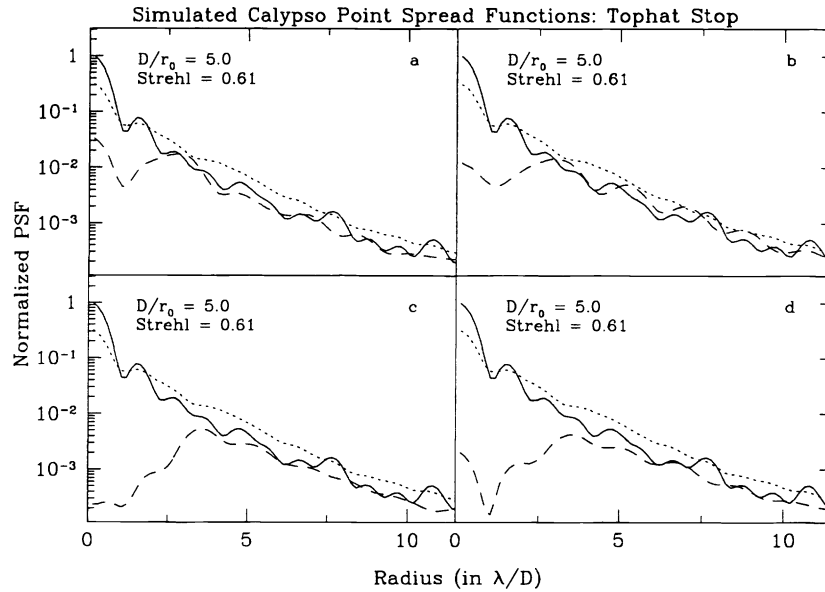
Figure 2. Azimuthally averaged PSFs for the 1.2m Calypso telescope, assuming 7 actuators across the pupil diameter ($\sim$ 38 total actuators) and occulting image-plane stops of $3\lambda/D$ (top row) and $6\lambda/D$ (bottom row), corresponding to 0.46 arcseconds and 0.92 arcseconds respectively at $\lambda = 0.9\mu m$. $\mathcal{F} = 0.25$ for figures in the left column, while $\mathcal{F} = 0.50$ for figures on the right. The AO-corrected PSF is signified by the solid line, while the $AO+$ coronagraph PSF is the dashed line. For comparison, we plot the PSF in the limit of no AO as the dotted line.

Simulated Palomar Point Spread Functions: Tophat Stop
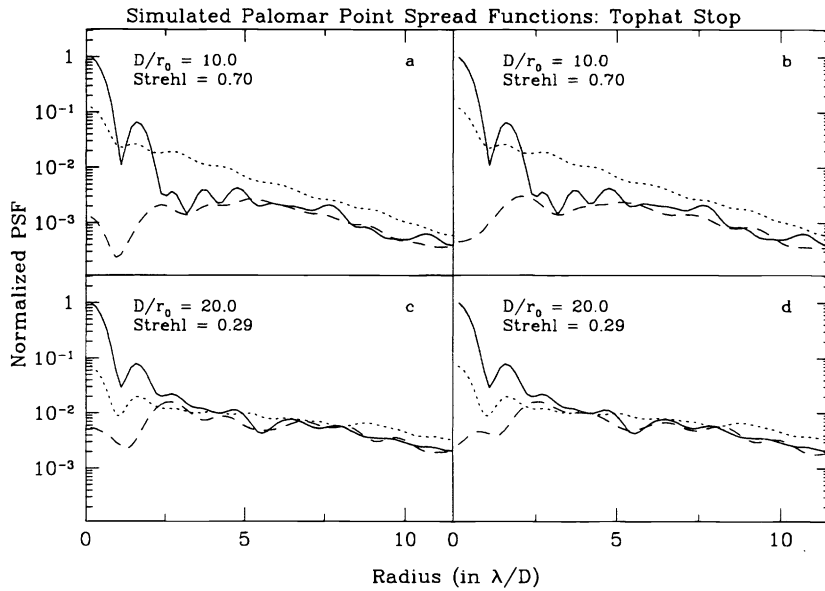
Figure 3. Azimuthally averaged PSFs for the Palomar Hale 5m telescope, assuming 16 actuators across the pupil diameter ($\sim$ 216 total actuators) and an occulting image-plane stop of $3\lambda/D$ (or 0.27 arcseconds at $\lambda = 2.2\mu m$). $\mathcal{F} = 0.25$ for figures in the left column, while $\mathcal{F} = 0.50$ for figures on the right. The AO-corrected PSF is signified by the solid line, while the $AO+$coronagraph PSF is the dashed line. For comparison, we plot the PSF in the limit of no AO as the dotted line.

406

Simulated Gemini Point Spread Functions: Tophat Stop
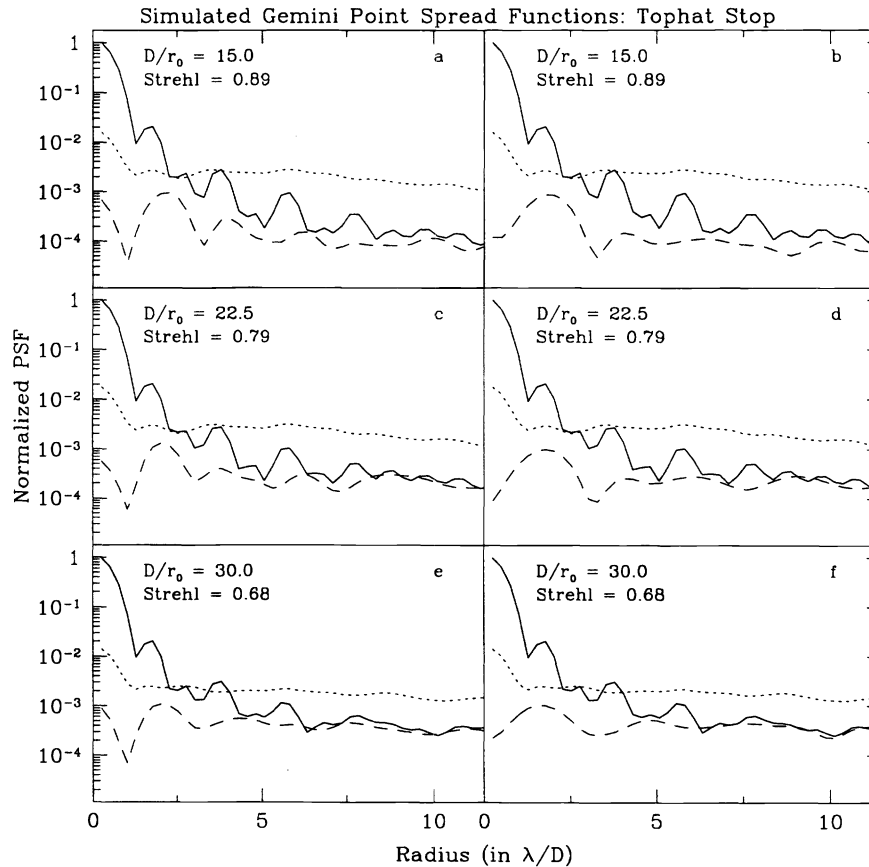
Figure 4. Azimuthally averaged PSFs for the 8.1m Gemini telescope, assuming 51 actuators across the pupil diameter ($\sim$ 2042 total actuators) and an occulting image-plane stop of $4\lambda/D$ (or 0.16 arcseconds at $\lambda = 1.6\mu m$). $\mathcal{F} = 0.25$ for figures in the left column, while $\mathcal{F} = 0.50$ for figures on the right. The AO-corrected PSF is signified by the solid line, while the $AO+$ coronagraph PSF is the dashed line. For comparison, we plot the PSF in the limit of no AO as the dotted line.
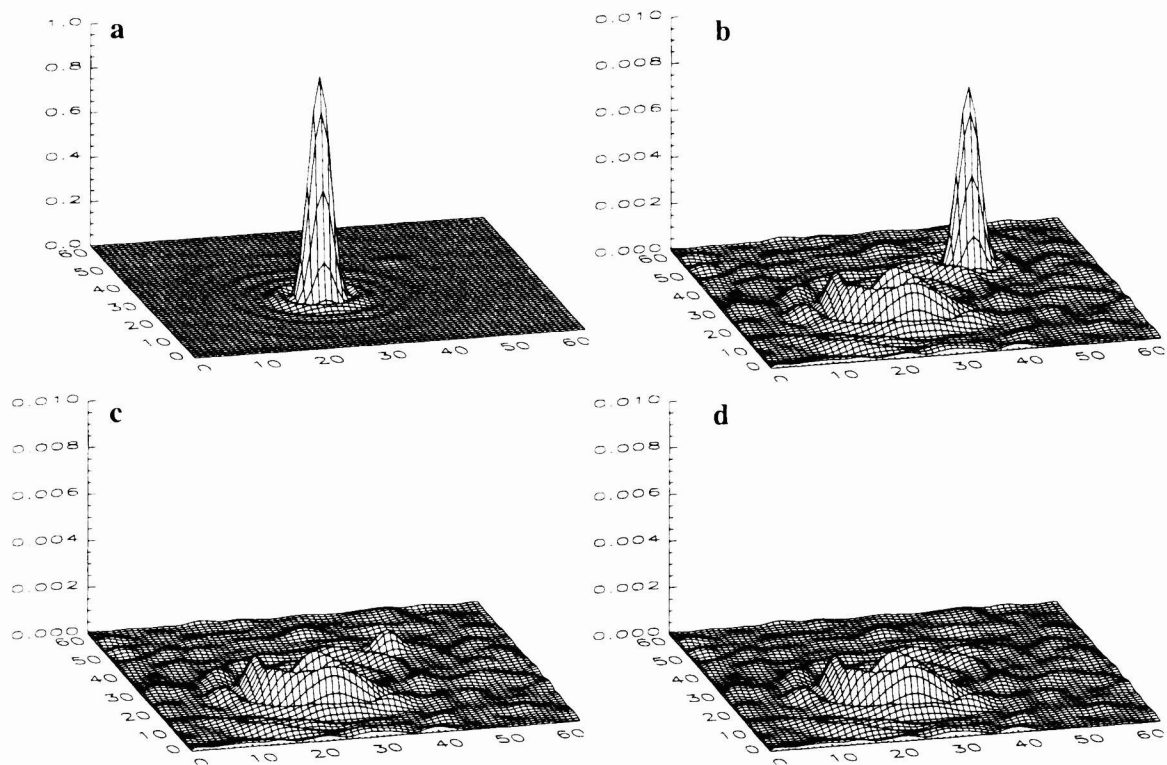
Figure 5. Realizations of star + faint companion at $4\lambda/D$ separation with $D/r_o = 15$ for the Gemini 8.1m telescope show the difference a coronagraph makes to faint companion detection. The primary star is located at (25,25), with a companion located at (42,42) in all frames. All realizations assume 2048 channels of AO, and have been normalized to the maximum value of the primary star's PSF. In (a), we show the primary star and a companion of $\Delta m = +5$ with no coronagraph in place. The companion is just visible in this figure. Figures (b), (c), and (d) exhibit companions of $\Delta m = +5$, $+7.5$ and $+10$ magnitudes respectively, with the primary occulted by an image-plane stop of diameter $4\lambda/D$ (0.16 arcsec in H). In (c), we see the object 7.5 magnitudes fainter than the primary is still discernible, though scattered light from the occulted primary is of comparable brightness. The $+10$ magnitude companion in (d) is not detectable above the scattered light present in this realization. We note that the companion's PSF is a scaled down version of the primary star's PSF with Lyot throughput losses accounted for. We expect the shape of the companion's PSF in this figure to be slightly different than that expected from an off-axis source imaged through the coronagraph.